Ocean Sci. Discuss., 8, 1215–1232, 2011
www.ocean-sci-discuss.net/8/1215/2011/
doi:10.5194/osd-8-1215-2011

Ocean Science Discussions

Sea surface temperature anomalies, seasonal cycle and trend regimes in the eastern Pacific coast

A. Ramos-Rodríguez[1], **D. B. Lluch-Cota**[1], **S. E. Lluch-Cota**[1], **and A. Trasviña-Castro**[2]

[1]Programa de Ecología Pesquera, Centro de Investigaciones Biológicas del Noroeste, S.C. La Paz, Mexico
[2]Departamento de Oceanografía Física-Unidad La Paz, Centro de Investigación Científica y Educación Superior de Ensenada, Ensenada, Mexico

Received: 10 May 2011 – Accepted: 15 May 2011 – Published: 25 May 2011

Correspondence to: A. Ramos-Rodríguez (jalejandro.ramos@gmail.com)

Published by Copernicus Publications on behalf of the European Geosciences Union.

Abstract

We used the extended reconstruction of sea surface temperature (ERSST) to analyze the variation of surface temperature and the seasonal cycle along the coast of the eastern Pacific (60° N–60° S, 61 pixels alongshore) from 1950 to 2010 (732 months). First we analyzed the monthly anomalies and looked for a relationship of such anomalies with total solar radiation (TSI) and then, the regime shift detector (RSD) was applied to detect possible temperature regimes in the series. Posterior to this, we calculated a yearly temperature range per pixel (amplitude of seasonal cycle) and through the subtraction of a latitudinal theoretical curve of temperature based on solar irradiance, the residuals of the seasonal cycle were obtained. The results showed an almost complete spatial synchrony and dominance of negative anomalies from 1950 to mid-late 1970's, with a switch to near-zero and positive anomalies in the late 1990's when a shift to negative values is detected. Such a shift lasted until the early 2000's when positive anomalies appear again but there is a change to negative anomalies in the late 2000's. These results were supported by the RSD. The TSI variability shows a clear relationship with that in sea surface temperature anomalies and with the regime changes. This would be due to a difference in the amount of energy received from the sun. Comparing two consecutive periods, 1952–1975 with 1977–1999, the second received 0.39 % more energy (approximately 3×10^8 J m^{-2}) from the sun. Seasonal cycles show larger range at northern latitudes (>40° N), northern tropical-template transition zone (20°–26° N) and in the tropical-equatorial band (0°–30° S). The smaller ranges occur at 0°–16° N and 50°–60° S. The residuals (seasonal minus the theoretical curve) indicate a clear modulation due to advection by ocean currents.

1 Introduction

In the late 1980's Lluch-Belda et al. (1989) reported an alternance between sardine and anchovy abundance in eastern boundary upwelling ecosystems (EBUE's) of the

OSD
8, 1215–1232, 2011

world. They proposed using the term "regime" when one species was dominating over the other, with a "regime shift" occurring when conditions changed to the opposite. The main cause for a warm/cold regime are related to warm/cool conditions in the surface ocean making the ecosystem more suitable for one of the two species (Lluch-Belda et al., 1992; Schwartzlose et al., 1999; Steele, 1998). Climate impact on individuals and populations may operate directly through physiology (metabolic and reproductive processes) or indirectly through the ecosystem, including prey, predators and competitors (Stenseth et al., 2002). This concept of regime was soon expanded to climatic factors and even to entire ecosystems and its components. It was also realized that regimes operate in different time scales, from inter-annual to decadal (Hare and Mantua, 2000; Meehl et al., 2003; Scheffer and Carpenter, 2003; Sandweiss et al., 2004). The oceans act as a climatic "thermostat" and the effect of climate variability on marine ecosystems can be traced through changes in sea surface temperature (SST, Stenseth et al., 2002). In this work we decided to study variability in coastal SSTs along the eastern Pacific Ocean, from 60° N to 60° S and from 1950 to 2010. The coastal region was chosen because most of the photosynthetic processes occur in coastal environments and are highly influenced by physical variables such as winds and currents, all of which have an effect on SSTs. Incoming radiation from the sun is the main source of energy and it is a fundamental measurement to understand terrestrial climate. Variations in the energy from the sun reaching the Earth's surface is often assumed a source of climate disparities (Reid, 1991). The spatial and temporal variation in solar radiation due to solar altitude, changes in Earth's orbital eccentricity and the tilt of planet's rotational axis produces seasonal variation in temperatures, precipitation and many other aspects of the atmospheric environment (Moran and Morgan, 1997). On longer time scales the radiation from the sun changes according to cycles of different lengths. Among them we can find the Sunspots or Schwabe cycle (11 yr; Dean, 2000), Hale cycles, (22 yr; Dean, 2000), Gleissberg cycles, (88 yr; Braun et al., 2005; Peristykh and Damon, 2003), DeVries-Suess cycles (210 yr; Wagner et al., 2001), Hallstat or Hallstadtzeit cycles (~2400 yr; Vasiliev and Dergachev, 2002; Charvátová, 2000).

OSD
8, 1215–1232, 2011

Such variability in the radiation from the sun, have an effect on the climate dynamics of the Earth and it is the main motor (Rind, 2002). Here we study the variability along the coast of the eastern Pacific, and we compare it with the variability in solar radiation. The hypothesis is that solar cycles should be present in records of different oceanographic variables modulated by other important processes such as the ocean currents. The work is organized as follows. The following section describes the data and methodology used for its analysis. Section 3 discusses our results and a final section is dedicated to summarize our findings and for the concluding remarks.

2 Methodology

2.1 Sea surface temperature data and total solar irradiance data

For SSTs we used the extended reconstruction of sea surface temperature data set (ERSST). This is a data base with a spatial resolution of 2-degrees and a time resolution of one month. It was generated from NOAA's Historical Merged Land-Ocean Surface Temperature Analysis, version 3b (http://www.esrl.noaa.gov/psd/data/gridded/data.noaa.ersst.html) and it includes data from January 1950 to December 2010, for a total of 732 months. The data in ERSST starts in 1854 but we decided to use only the above-mentioned period because the reported confidence interval for uncertainty for the quasi-global average for 1950 onwards is of 0.1 °C. Improved fit procedures are also included for this period along with the omission of satellite observations due to the larger residual bias of such observations (Smith and Reynolds, 2003, 2004; Smith et al., 2008). For the analysis we selected the pixels from 60° N–60° S nearest to the coastline (61 pixels in total). The total solar irradiance data (TSI) was obtained from the SOLARIS working group web page hosted by the Physics of the Middle Atmosphere Group of the Freie Universität of Berlin (http://www.geo.fu-berlin.de/en/met/ag/strat/forschung/SOLARIS/Input_data/). Here they include data for the period 1880–2004. Such data is calculated with the use of observational data and proxies. It includes

OSD
8, 1215–1232, 2011

corrections for wavelength-dependent degradation common to measurements of TSI. A more detailed description of these estimates can be found in Lean et al. (1997), Lean (2000) and Lean et al. (2005). To determine the exact length and timing of every cycle the cyclic descent method was used (Bloomfield, 1976). The latter method is useful to define the cycles present within a time series and fits a polynomial model that can be employed to forecast.

2.2 Monthly anomaly analysis

To calculate the monthly anomalies for each 2° by 2° coastal pixel we first obtained a mean of all months in the database to obtain the annual mean time series. This was then subtracted from individual monthly values in the time series. In order to detect the presence of a regime shift in the different time series we used the Regime Shift Detector (RSD, Rodionov, 2004; Rodionov and Overland, 2005). The RSD is a useful tool to detect abrupt changes in either the mean or variance within a time series trough an statistical test (t-test), and have the advantage to detect a shift with a minimum delay and not to be biased by long intervals when the observations remain above or below the overall mean value (red noise). Here the RSD was used with a significance level of 90 % ($p < 0.1$), cut-off length of 60 month and Huber's weight parameter of 1. For the red-noise estimation, the inverse proportionality with 4 corrections (IP4) method was selected, using a sub-sample size of 39. Before applying the RSD a data pre-whitening was carried out (Rodionov, 2006). With the parameters above mentioned, we expect this method will detect a regime shift at least 5 yr long.

2.3 Seasonal amplitude cycle analysis

Changes in the seasonal cycle are studied from yearly amplitudes obtained for every year in the data base. To calculate the deviations from the amplitude of seasonal cycle we computed for every pixel the annual mean solar irradiance. The latter varies due to the solar altitude, latitude and net irradiance throughout the year. Then, with the solar

OSD
8, 1215–1232, 2011

irradiance data we calculated the amplitude of the solar irradiance for every pixel to obtain the theoretical curve of solar irradiance amplitude, which was used to compute regressions vs. the mean seasonal amplitude to obtain a theoretical curve of latitudinal SST amplitude based on solar radiation.

3 Results and discussion

3.1 Meridional coastal variability: mean seasonal SST cycle and theoretical seasonal cycle based on solar irradiance curve

Figure 1a compares the annual mean SST range with the theoretical seasonal temperature amplitude obtained from the irradiance cycle. This is shown for all coastal stations along the eastern Pacific. The range was calculated for every year in the data base, as the yearly (maximum–minimum) temperature. From 60° to 56° N in the region of the Alaska current the seasonal cycle is 0.6 to 1 °C larger than the theoretical curve (TC) this is because this current is relatively warm and tends to increase the amplitude of the seasonal cycle. From 54° to 46° N the mean SST range is close to the TC with differences less than 0.47 °C, most of them above the TC. This is thought to occur here because this region does not have coastal upwelling sites and the California Current is found far from the coast. From 44° to 30° N is an area influenced by both the California Current and coastal upwelling. Consequently, the range is below the TC (0.45–1.5 °C) with smaller differences in the latitudinal band 36°–34° N. From 20° to 26° N the range of SST is above that of the TC with values ranging from 1 to 2 °C and the largest differences are found at 26° to 24° N. Here the increase in seasonal range is due to the influence of tropical waters in the late summer and the presence of either the California Current or coastal upwelling lowering the coastal SSTs most of the year. The latitudinal band from 18° to 2° N includes the eastern Pacific warm pool and north equatorial region. This shows values close to the TC with differences no larger than 0.5 °C. To the south, from the Equator to 28° S we find the Humboldt or Peru current region and

OSD
8, 1215–1232, 2011

intense coastal upwelling. Consequently the range is above the TC (values between 0.8–5.1 °C) with largest differences in the upwelling region between 4° and 12° S (4 to 5.1 °C). From 30° S to the South the mean SST range diminished progressively southwards. Values here are always lower than the TC: at 42° S the annual range is 1.2 °C smaller that the TC and at 58° S is 5.15 °C smaller that the TC. This is attributed to the influence of the circumpolar current and its extension to the north along the American coast (see also Sect. 3.3). Mean SSTs show a latitudinal gradient (Fig. 1b) with cooler temperatures at higher latitudes (coolest at 60° S, 4.1 °C), as expected, and warmer temperatures near the equator with the warmest north of the equatorial region, from the 6°–18° N (27–28.5 °C) including the coast of the eastern Pacific warm pool (~6°–14° N).

3.2 SST monthly mean anomalies, solar irradiance and regime shift detector (RSD)

Figure 2 shows the time series for the total solar irradiance (Fig. 2a), the Hovmöller diagram (latitude vs. time) of the SST monthly anomalies (Fig. 2b) and the Hovmöller diagram of the RSD applied to every SST anomalies time series (Fig. 2c). Total solar irradiance (TSI) data (Fig. 2a) shows 4 full-cycles for the period studied. To determine the exact length and timing of every cycle the Cyclic Descent Method was used (described in the methods section). This method is useful to define the cycles present within a time series and fits a polynomial model that can be employed to forecast the behavior of a periodic component of the signal (Fig. 2a, blue line, $R^2 = 0.78$). The position of the start/end of each cycle is determined using this method and in the figure is marked by black horizontal lines. TSI series begin with the end of a previous period (1950–1953) and then the signal contains an 11.5-yr cycle from January 1954 to July 1964. This cycle has a minimum/maximum irradiance value of 1365.5/1367.5. This is followed by a longer (12-yr) cycle from August 1964–July 1975. This is also the cycle with the lowest irradiance of the whole TSI series with minimum/maximum values of 1365.3/1366.3. The next two cycles last 11.5 and 11 yr, respectively. The first one

OSD
8, 1215–1232, 2011

goes from July 1975 to December 1985 and the second from January 1986 to February 1996. The minima and maxima for both cycles are almost identical, around 1365.4 and 1367.1, respectively. The remaining portion of series is an incomplete period of increasing trend. In the following two panels of the figure we show the SST anomalies and the regime shift detector applied to it. Negative values of the SST (Fig. 2b) anomalies dominate the period of 1950 to 1978 (regime 1 in Fig. 2c). Zero and positive anomalies dominate from 1979 to 1999 (regime 2 in Fig. 2c) and mostly weak anomalies from 2000 onwards (regime 3 in Fig. 2c). During first regime negative anomalies of 2 °C are common and only during El Niño southern oscillation (ENSO) events (1957–1958, 1965–1966, 1968–1969, 1972–1973, 1976–1977) is that near-zero or positive anomalies can be observed. During each ENSO the intensity of the anomaly and its zonal extent are an indication of the strength of individual occurrences. In most ENSO events, positive anomalies in the Southern Hemisphere range from the equator to about 16° S. However, during some of the more intense ENSO events (v.g. 1957–1958) positive anomalies extend poleward to 30° S and to 60° N. Mid-intensity ENSO events result in a weaker response in the Northern Hemisphere. During regime 2 (warm), from 1979 to about 1999, there is a clear dominance of near zero to positive anomalies with the only exception of the negative anomalies associated to negative ENSO (La Niña) events. The strongest ENSO events of the whole series occur during this warm regime, for instance the 1982–1985 and 1997–2000 events. Such events have the widest zonal extent. In the 1997–1998 event, positive anomalies were recorded along the coast from 56° S to 60° N. The second regime shift occurs around 1998–1999, after the strongest ENSO in this record. First, a shift back towards negative anomalies occurs, lasting about 6 yr. Then a brief near-zero to warm-anomaly period occurs in 2003 only to switch again to negative anomalies from 2007–2008. The main features of this period are (a) the weak character of the anomalies throughout the coastal region and (b) the lack of strong ENSO events. These brief and weak events are similar to the El Niño-Modoki class of ENSO events. Such behavior has been described as a consequence of climate change by Ashok and Yamagata (2009). The behavior of the total solar

OSD
8, 1215–1232, 2011

irradiance curve (Fig. 2a) is consistent with the regimes described by the SST anomaly curves (Fig. 2b). During the cool regime (1950 to 1978, as seen in Fig. 2b and c) two full solar radiation cycles take place. The first cycle is short and reaches the highest TSI values of the two. The second is an elongated cycle with comparatively lower TSI maximum. This shows a clear relationship with the SST anomalies. The maximum of the first cycle occurs during the El Niño 1957–1958 and during 1964–1975 the TSI reaches a minimum and the period is dominated by negative anomalies. This TSI cycle is also the longest of the whole series, lasting 12 yr in total. As pointed out by Friis-Christensen and Lassen (1991) longer sunspot cycles have a relationship with cooler temperatures on the planet due to weaker solar activity. Calculating the area under the TSI cycle curves also helps in comparing successive regimes. The difference between the area below the TSI curves of the first and second regimes is of about 3×10^8 J m^{-2}. This is equivalent to about 0.39 % more energy received during the warm period compared to the cool period. This is a significant value. Variations in total solar energetic output, as determined over time scales for which reliable climatic data are available, are small (less than about 0.1 %). Such percentage corresponds to a change of irradiance of approximately 1 W m^{-2} outside the atmosphere (or 0.2 W m^{-2} averaged over Earth's surface) between periods of maximum and minimum activity and over a full solar cycle (see for instance Haigh, 1996). Furthermore, peaks in solar forcing increase the energy input to the upper ocean, increasing the latent heat flux (moisture) into the atmosphere, and moisture produced this way is carried by the trade winds towards the convergence zones where precipitation occurs. This intensified precipitation strengthens the Hadley and Walker circulations in the troposphere, with an associated increase in trade wind strength capable of increasing the strength of equatorial ocean upwelling and of lowering equatorial SSTs (Meehl et al., 2009). The regime shift detector (RSD) is applied to the SST anomalies (Fig. 2c). What makes this method useful is the use of a statistical test which includes a measure of the level of significance. This is very useful to detect if there is meaningful change in the mean or variance of the time series. The Hovmöller diagram of the RSD corroborates what was previously stated (Fig. 2c).

OSD
8, 1215–1232, 2011

There was a basin-scale regime shift about 1978 from cooler to warmer conditions. This regime shift occurs along the whole basin, with the exception of the region from 4° S to 16°–18° N where the regime shifts happened a little later, in the mid-1980's. The warm event from 24° S to 60° N in late 1950's is related to the occurrence of the 1957–1958 ENSO event. The warmer regions during the positive regime occur from 20° S to 28° N and North of 28° N only during the 1990's. Warmer values of the RSD around 20° S during this regime are a consequence of ENSO events. The regime changes to cool conditions in the late 1990's. This occurs along the whole basin and it might have been triggered by La Niña 1999–2001. This event started in late 1998 and lasted through 2000 with negative anomalies observed even during 2001.

3.3 Seasonal cycle amplitude and RSD

The Hovmöller diagram of the temperature amplitude (TA) and temperature residual (TR = range – theoretical curve of solar radiation, TC, see the methods section) are shown in Fig. 3a and b, respectively. TA in Fig. 3a clearly denotes a latitudinal gradient and most of its zonal variation can be explained by the SST mean latitudinal range (Fig. 1a). TA is always larger than 7 °C in the mid- to high-latitudes (from 40° N northwards), diminishes to a minimum of 2–4 °C from 28° to 40° N, increases again in the tropical transition (from 20° to 26° N) and in the tropical to equatorial band the range is very small (less than 3 °C). In the Southern Hemisphere the larger ranges occur in the equatorial to subtropical band (south of 0° to 26° S) reaching up to 10 °C. Only the extreme south shows again a small range similar to that observed in the equator. It is worth noting that ENSO events have a strong effect over the seasonal cycle, amplifying it or reducing it. For example in the El Niño 1997–1998 the effect differs along the coast. From the equator southwards to 30° S the interaction with the Humboldt current results in a reduction of the TA of about 2 to 3 °C. Northwards along the coast the TA is amplified in the subtropical to tropical transition (20° to 26° N) and in the mid- to high-latitude (40° N and northwards) due to the poleward propagation. After El Niño, La Niña acts in exactly the opposite way, it amplifies the range southwards

OSD
8, 1215–1232, 2011

of the Equator and it reduces the TA northwards. When subtracting the TC from the TA (Fig. 3b) the residuals (TR) indicate how the temperature range is affected by other factors than merely solar radiation. Physical factors such as ocean currents are considered as having the greater importance. The southernmost portion shows the lowest negative residuals (−5 to −7 °C) and lowest temperatures (around 5 °C) as an influence of the Antarctic circumpolar current. This indicates that seasonal cycle is shorter than expected, being this zone colder than the TC and homogeneous all year long. Northwards, there is a transitional zone among this current and the Humboldt current (also known as Peru Current) located approximately from 50° to 26° S (temperature ~10–17 °C). The residuals here are between 0 and −4 °C, which indicates that this zone is still cooler than expected and that it has a reduced seasonal cycle. Between 24° S and the Equator residuals are positive and reach the highest values. This zone is influenced by the Humboldt Current. This region has a greater seasonal cycle than expected due to these currents are usually considered cold currents and also due to seasonal coastal upwelling. From 2° to 18° N the residuals are the smallest and slightly negative (> −2 °C) indicating that this region has seasonal cycle smaller than the TC. This is the warmest coastal region in the eastern Pacific coast with a mean SST around ~27–28 °C and it is where the eastern Pacific Warm Pool is located. This zone is relatively stable as a consequence of the lack of a dominant large-scale circulation and high solar radiation. In the 20°–26° N region, the seasonal cycle is amplified by almost 2 °C in the region where the California Current seasonally nears the coast. This region includes the transition between tropical and template climates but still receives a large amount of solar radiation, with the Tropic of Cancer located at ~23°26′16″ N. All these condition result in a marked seasonality. From 28° to ~44° N the seasonal cycle is lower than expected (−2 °C) basically due to the combined effect of the North Pacific Current in the north, the California Current and seasonal coastal upwelling which helps in maintaining low SSTs. The northernmost region (46°–60° N) is characterized for a seasonal cycle slightly larger than expected (up to ~2 °C), although it shows variability with the dominance of negative values in some periods. This is because this zone is influenced

OSD
8, 1215–1232, 2011

by the Alaska current, considered as a warm current, and this interannual range variability reflects its variability near the coast. The RSD applied to TA and TR (figure not shown) showed no discernible patterns, as was the case for SST monthly anomalies. The ocean currents play an important role in the distribution of heat and momentum in the earth; in this case they alter the SST range near the coast as evidence of the power of the currents to distributing energy received to other latitudes.

4 Conclusions

In the last 61 yr two shifts to different "temperature regimes" were detected along the coast of the eastern Pacific. This was accomplished through the analysis of SST monthly anomalies and using statistical tools, such as the regime shift detector (RSD). Such regimes are clearly related to the solar activity, particularly to the amount of TSI and length and intensity of sunspot cycle. Noteworthy is the relationship observed between TSI and SST: more energy was received at the top of the atmosphere during the warm than in the cool regime. As stated, the difference between regimes is $3 \times 10^8\,\mathrm{J\,m^{-2}}$. This is equivalent to about 0.39 % more energy received during the warm period compared to the cool period. Although a great percentage of the energy received at the top of the atmosphere is lost due to dispersion, refraction, reflection etc. the remaining energy enters the climate system and the loss of about 0.39 % during the cool regime is not a negligible amount. Another evidence of the influence of the incoming radiation from the sun in the climatic regimes is that during the cool regime the length of radiations cycles is longer (11.5 and 12 yr each) than the remaining two cycles in the series (11.5 and 11 yr each). And the second cycle of the cool regime (1964–1975) received the least amount of energy of the series. So probably these combined factors, less energy received due to reduced solar activity because longer cycles and less irradiance, caused the dominance of negative anomalies in the first ~30 yr on earth. The opposite happens in the next two cycles, more TSI and shorter sunspot cycles. It is believed that these are important features that cannot be ignored

OSD
8, 1215–1232, 2011

and should be considered as a partial evidence of the relationship sun-climate. Although the connection between TSI and climate is much more complex than just a direct relationship among TSI and temperature is clearly recognized that as solar activity is the main factor which drives climate on earth, and its importance cannot be denied. The seasonal cycle in the Ocean Pacific eastern coast has not significantly changed in the 61-year period studied. We did find that some climatic variability, such as ENSO events, is capable of altering the amplitude of the seasonal cycle. And its effect is superimposed on the long-term climatic alterations. Also, the seasonal cycle in coastal regions are influenced also by the advection of heat by the oceanic currents. They play an important role in the modulation of the amplitude of seasonal cycle in coastal areas.

Acknowledgements. The first author wants to thank to Consejo Nacional de Ciencia y Tecnología (CONACyT) for the scholarship 48486. ATC, SELC and DBLC are SNI grant holders. We also want to thank to Miguel Angel Cosío for his valuable comments about the present work.

References

Ashok, K. and Yamagata, T.: The El Niño with a difference, Nature, 461, 481–484, 2009. 1222

Bloomfield, P.: Fourier Analysis of Time Series: An Introduction, Wiley Series in Probability and Mathematical Statistics, John Wiley & Sons, 1st edn., 1976. 1219

Braun, H., Christl, M., Rahmstorf, S., Ganopolski, A., Mangini, A., Kubatzki, C., Roth, K., and Kromer, B.: Possible solar origin of the 1,470-year glacial climate cycle demonstrated in a coupled model, Nature, 438, 208–211, 2005. 1217

Charvátová, I.: Can origin of the 2400-year cycle of solar activity be caused by solar inertial motion?, Ann. Geophys., 18, 399–405, doi:10.1007/s00585-000-0399-x, 2000. 1217

Dean, W. E.: Sun and climate, USGS Fact Sheet FS-095-00, 2000. 1217

Friis-Christensen, E. and Lassen, K.: Length of the Solar Cycle: An Indicator of Solar Activity Closely Associated with Climate, Science, 254, 698–700, 1991. 1223

Haigh, J. D.: The impact of solar variability on climate, Science, 272, 981–984, 1996. 1223

OSD

8, 1215–1232, 2011

Hare, S. R. and Mantua, N. J.: Empirical evidence for North Pacific regime shifts in 1977 and 1989, Prog. Oceanogr., 47, 103–145, 2000. 1217
Lean, J.: Evolution of the Sun's spectral irradiance since the maunder minimum, Geophys. Res. Lett., 27, 2425–2428, 2000. 1219
Lean, J., Rottman, G. J., Harder, J., and Kopp, G.: Sorce contributions to new understanding of global change and solar variability, Sol. Phys., 230, 27–53, 2005. 1219
Lean, J. L., Rottman, G. J., Kyle, H. L., Woods, T. N., Hickey, J. R., and Puga, L. C.: Detection and parameterization of variations in solar mid- and near-ultraviolet radiation (200–400 nm), J. Geophys. Res., 102, 29939–29956, 1997. 1219
Lluch-Belda, D., Crawford, R., Kawasaki, T., MacCall, A., Parrish, R., Schwartzlose, R. A., and Smith, P. E.: World-wide fluctuations of sardine and anchovy stocks: The Regime Problem, S. Afr. J. Marine Sci., 8, 195–205, 1989. 1216
Lluch-Belda, D., Hernandez-Vazquez, S., Lluch-Cota, D. B., Salinas-Zavala, C. A., and Schwartzlose, R. A.: The recovery of the California Sardine as related to global change, Cal. Coop. Ocean. Fish., 33, 50–59, 1992. 1217
Meehl, G. A., Washington, W. M., Wigley, T. M. L., Arblaster, J. M., and Dai, A.: Solar and greenhouse gas forcing and climate response in the twentieth century, J. Climate, 16, 426–444, 2003. 1217
Meehl, G. A., Arblaster, J. M., Matthes, K., Sassi, F., and Loon, H. v.: Amplifying the Pacific climate system response to a small 11-year solar cycle forcing, Science, 325, 1114–1118, 2009. 1223
Moran, J. M. and Morgan, M. D.: Meterology: The atmosphere and science of weather, Prentice-Hall, Inc., Upper Saddle River, New Jersey, 5th edn., 1997. 1217
Peristykh, A. N. and Damon, P. E.: Persistence of the Gleissberg 88-year solar cycle over the last 12,000 years: Evidence from cosmogenic isotopes, J. Geophys. Res., 108, 1–15, 2003. 1217
Reid, G. C.: Solar total irradiance variations and the global sea surface remperature record, J. Geophys. Res., 96, 2835–2844, 1991. 1217
Rind, D.: The Sun's role in climate variations, Science, 296, 673–677, 2002. 1218
Rodionov, S.: A sequential algorithm for testing climate regime shifts, Geophys. Res. Lett., 31, L09204, doi:10.1029/2004GL019448, 2004. 1219
Rodionov, S.: Use of prewhitening in climate regime shift detection, Geophys. Res. Lett., 33, L12707, doi:10.1029/2006GL025904, 2006. 1219

OSD
8, 1215–1232, 2011

Rodionov, S. and Overland, J. E.: Application of a sequential regime shift detection method to the Bering Sea ecosystem, ICES J. Mar. Sci., 62, 328–332, 2005. 1219
Sandweiss, D. H., Maasch, K. A., Chai, F., Andrus, C. F. T., and Reitzf, E. J.: Geoarchaeological evidence for multidecadal natural climatic variability and ancient Peruvian fisheries, Quaternary Res., 60, 330–334, 2004. 1217
Scheffer, M. and Carpenter, S. R.: Catastrophic regime shifts in ecosystems: linking theory to observation, Trends Ecol. Evol., 18, 648–656, 2003. 1217
Schwartzlose, R., Alheit, J., Bakun, A., Baumgartner, T., Cloete, R., Crawford, R., Fletcher, W., Green-Ruiz, Y., Hagen, E., Kawasaki, T., Lluch-Belda, D., Lluch-Cota, S., MacCall, A., Matsuura, Y., Nevarez-Martinez, M., Parrish, R., Roy, C., Serra, R., Shust, K., Ward, M., and Zuzunaga, J.: Worlwide large-scale fluctuations of sardine and anchovy populations, S. Afr. J. Marine Sci., 21, 289–347, 1999. 1217
Smith, T. M. and Reynolds, R. W.: Extended reconstruction of global sea surface remperatures based on COADS data (1854–1997), J. Climate, 16, 1495–1510, 2003. 1218
Smith, T. M. and Reynolds, R. W.: Improved Extended Reconstruction of SST (1854–1997), J. Climate, 17, 2466–2477, 2004. 1218
Smith, T. M., Reynolds, R. W., Peterson, T. C., and Lawrimore, J.: Improvements to NOAA's historical merged land-ocean surface temperature analysis (1880–2006), J. Climate, 21, 2283–2296, 2008. 1218
Steele, J. H.: Regime shifts in marine ecosystems, Ecol. Appl., 8, S33–S36, 1998. 1217
Stenseth, N. C., Mysterud, A., Ottersen, G., Hurrell, J. W., Chan, K., and Lima, M.: Ecological effects of climate fluctuations, Science, 297, 1292–1296, 2002. 1217
Vasiliev, S. S. and Dergachev, V. A.: The ~ 2400-year cycle in atmospheric radiocarbon concentration: bispectrum of 14C data over the last 8000 years, Ann. Geophys., 20, 115–120, doi:10.5194/angeo-20-115-2002, 2002. 1217
Wagner, G., Beer, J., Masarik, J., Muscheler, R., Kubik, P. W., Mende, W., Laj, C., Raisbeck, G. M., and Yiou, F.: Presence of the solar de Vries cycle (~205 years) during the last ice age, J. Geophys. Res., 2, 303–306, 2001. 1217

OSD
8, 1215–1232, 2011

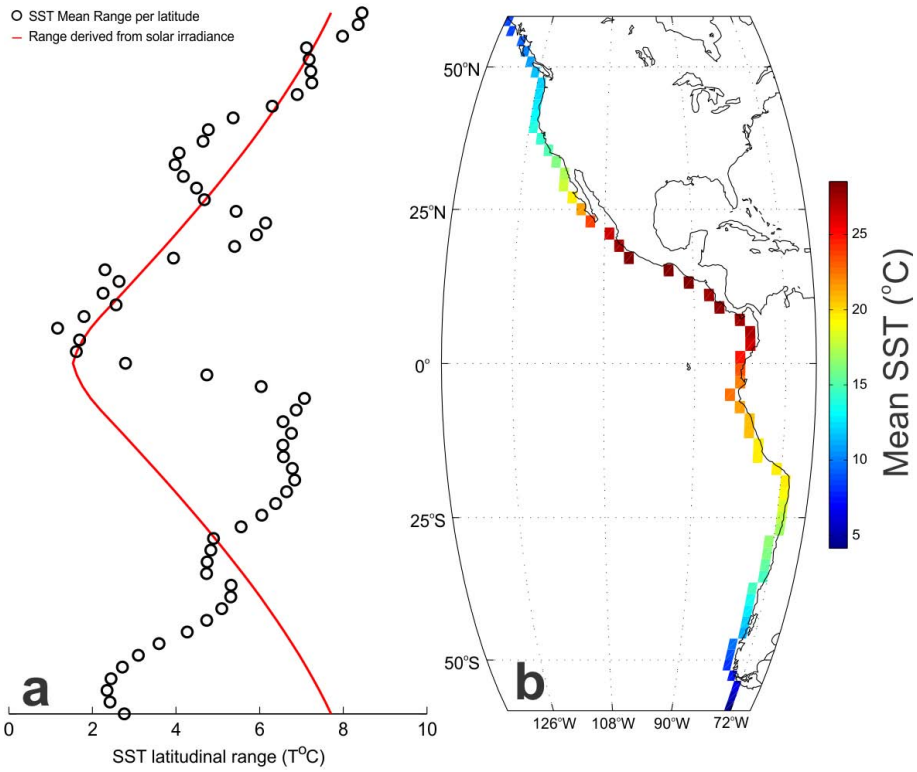

Fig. 1. (a) Mean latitudinal SST range for the selected pixels for the same period (black circles) and the theoretical SST range derived from solar irradiance (red line). **(b)** Coastal stations (pixels) selected for the study with their mean SST for the 61 yr in the data base.

OSD
8, 1215–1232, 2011

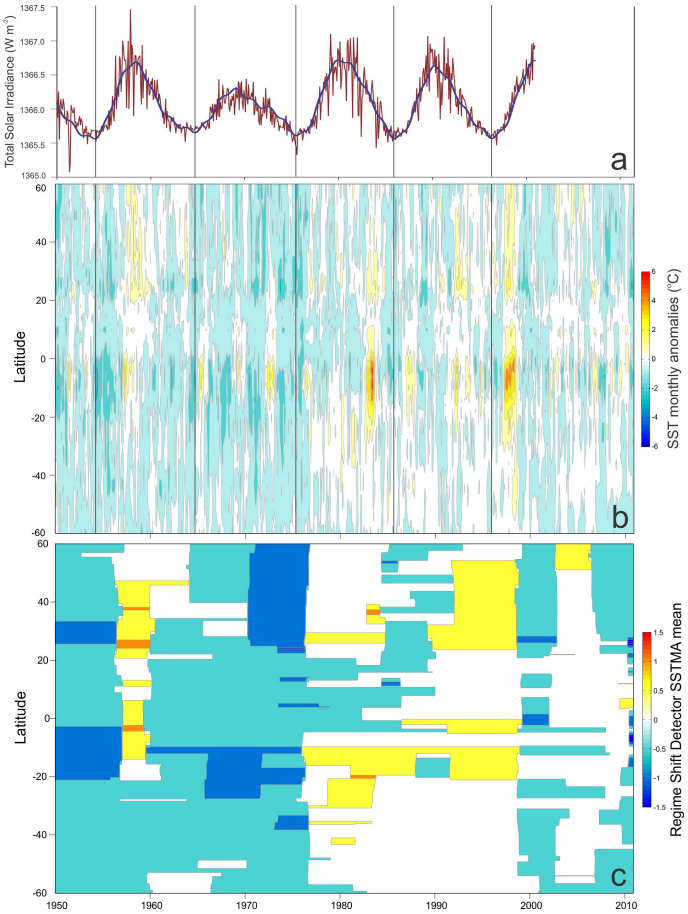

Fig. 2. Total solar radiation **(a)**, Hovmöller diagram of the SST monthly anomalies **(b)** and the same type of diagram for RSD applied to SST monthly anomalies **(c)**.

OSD
8, 1215–1232, 2011

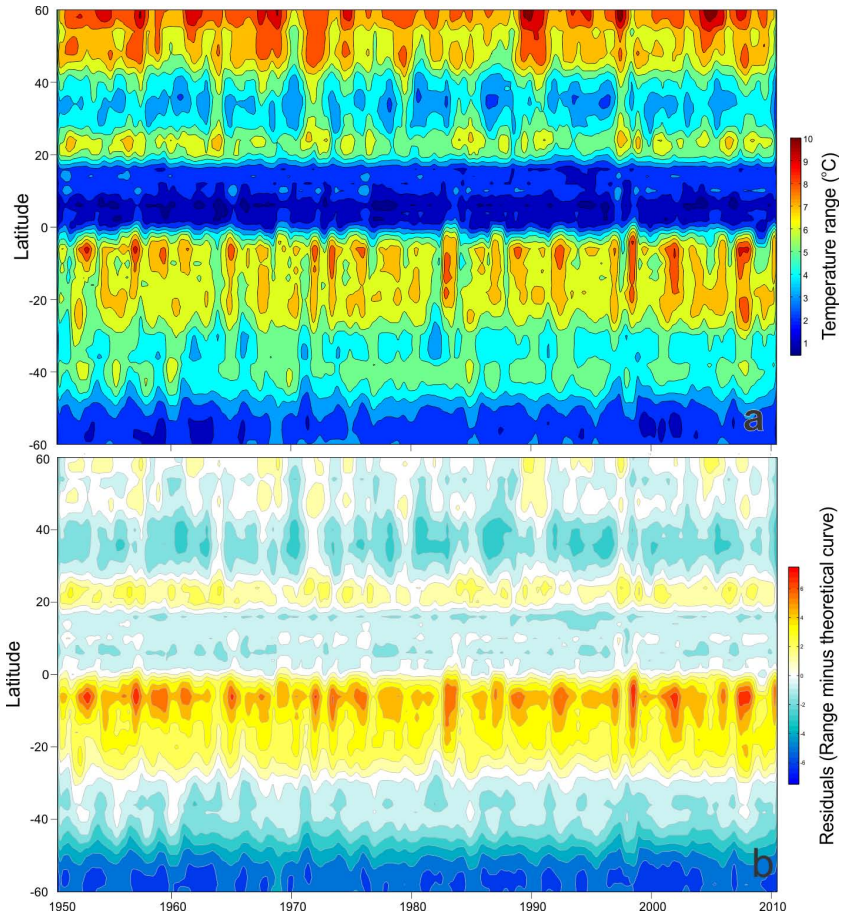

Fig. 3. Hovmöller diagram of the SST range (TA, **a**), and the residuals (TR) calculated from subtracting the theoretical curve from the range **(b)**.

OSD
8, 1215–1232, 2011